Proceedings of the 2009 ASME Joint Rail Conference
JRC2009
March 3–5, 2009

JRC2009-63054

MODELING MATERIAL FAILURE DURING CAB CAR END FRAME IMPACT

Richard Stringfellow
Christopher Paetsch
TIAX LLC
Cambridge, Massachusetts, USA

ABSTRACT

New standards have been proposed to increase the strength requirements for cab car end structures and impose further requirements on their ability to absorb energy during a grade-crossing collision [1, 2]. To aid in the development of these new standards, the Federal Railroad Administration (FRA) and the Volpe Center recently completed a set of full-scale tests aimed at assessing the quasi-static and dynamic crush behavior of these end structures.

In support of this testing program, end frames designed to meet the new standards were fabricated and retrofitted onto the forward end of an existing cab car. A series of large-deformation quasi-static and explicit dynamic finite element analyses (FEAs) were performed to evaluate the performance of the design.

Based on the results of a 2002 full-scale test in which a heavy steel coil impacted the corner post of an end frame built to these new standards, some fracture was expected in certain key end frame components during the tests. For this reason, a material failure model, based on the Bao-Wierzbicki fracture criterion [3], was implemented in the FEA model of the cab car end frame using ABAQUS/Explicit. The FEA model with material failure was used to assess the effect of fracture on the deformation behavior of cab car end structures during quasi-static loading and dynamic impact and, in particular, the ability of such structures to absorb energy.

The failure model was implemented in ABAQUS/Explicit for use with shell elements. A series of preliminary calculations were first conducted to assess the effects of element type and mesh refinement on the deformation and fracture behavior of structures similar to those found on cab car end frames, and to demonstrate that the Bao-Wierzbicki failure model can be effectively applied using shell elements.

Model parameters were validated through comparison to the results of the 2002 test. Material strength and failure parameters were derived from test data for A710 steel. The model was then used to simulate the three full-scale tests that were conducted during 2008 as part of the FRA program: a collision post impact, and quasi-static loading of both a collision post and a corner post. Analysis of the results of the two collision post tests revealed the need for revisions to both the design of some key end frame components and to key material failure parameters. Using the revised model, pre-test predictions for the outcome of the corner post test were found to be in very good agreement with test results.

INTRODUCTION

The Federal Railroad Administration (FRA), with the assistance of the Volpe Center, is engaged in active research aimed at increasing the safety of passenger train occupants. As part of this research, FRA is proposing amendments to regulations governing the structural behavior of the front end of cab cars and multiple-unit locomotives [1]. In addition to numerous requirements for the strength of key end frame components, the proposed regulations impose requirements for energy absorption and post deformation, following recommendations of the American Public Transportation Association (APTA) [2].

The proposed rule provides two alternative testing methods for demonstrating absorption of collision energy. Following the quasi-static method, the front end structure must be capable of absorbing a specific amount of energy (135,000 ft-lb for a load applied to the collision post, and 120,000 ft-lb for a load applied to the corner post). Following the dynamic method, the structure must be capable of withstanding a longitudinal impact of a proxy object that imparts the same respective amount of energy. For example, for a 14,000 lbm proxy object impacting a 70,000 lbm vehicle, the impact speed must be at least 18.2 mph for the collision post test or 17.1 mph for the corner post test. In both the quasi-static and dynamic test scenarios, the load is applied approximately 30 inches above the underframe. No more than 10 inches of longitudinal permanent deformation into the occupied volume is allowed. Some fracture is permitted, as long as the post does not completely separate from the end frame.

In an earlier program contracted by the Volpe Center and FRA [4], a design was developed for a cab car end frame that

satisfies Federal regulations that were introduced in 1999. This state-of-the-art (SOA) end frame was fabricated and retrofitted onto existing cab cars for full-scale testing.

A dynamic impact test of the corner post of the SOA end frame was conducted at FRA's Transportation Technology Center (TTC) in June 2002. The results of the test indicated that the SOA end frame was a substantial improvement to a design built to pre-1999 Federal regulations (1990's design) [5], with the corner post remaining attached at its connections following the test. However, there were a few locations at which material failure was observed, including the attachment of the corner post to the end beam.

To further evaluate the proposed rules and test methods described above, the Volpe Center recently conducted three additional full-scale tests of the SOA end frame. A dynamic test of a heavy cart impacting the collision post was conducted in April 2008 [6]. Quasi-static tests, in which the end frame was loaded at a collision post and at a corner post, were conducted in June and August 2008, respectively. The work described in this paper was conducted in support of this testing program.

Finite element analyses (FEAs) were used to guide the design of the end frame retrofit onto an existing cab car, determine if the design satisfied the structural requirements imposed by the new rules, and predict the outcome of the recent full-scale tests. With the knowledge that material failure was observed in the 2002 corner post impact test, a material failure model was incorporated into the finite element models with the aim of improving the accuracy of model predictions.

Material failure models were recently used with great success to model the impact of a railroad tank car with a rigid punch [7–10]. These failure models employ the Bao-Wierzbicki fracture criterion [3], which features a specific stress triaxiality dependence on the plastic strain for initiation of failure. In the analyses, the material failure models were implemented for use with three-dimensional solid elements. Despite the fact that the tanks are thin-walled, it was found that solid elements were required to accurately capture the local deformation and failure processes associated with the penetration of the punch through the wall of the tank. Since solid elements are computationally much more 'expensive' than shell elements, an ABAQUS feature called shell-to-solid coupling was employed so solid elements in the region of fracture could be used, and shell elements throughout the remainder of the railroad car tank, greatly reducing the computational requirements for the analyses.

A considerable model development effort was undertaken to first evaluate the use of mixed solid/shell element models, with shell-to-solid coupling, and then shell element-only models. Ultimately, certain features of the cab car end frame impact problem made the use of shell-only models more attractive, and these were used for the remainder of the analyses.

The model was then validated through comparison to the results of the 2002 corner post impact test. Certain key model parameters were adjusted to provide an optimal fit to test relevant test results.

The validated model was then used to predict the outcome of the April 2008 dynamic impact test in which a collision post was impacted by a 14,000 lbm cart with a coil-shaped indenter at its leading end. The results of the model predictions were compared with analysis results. While there was a reasonable level of agreement between the model predictions and the outcome of the test, some aspects of the test were not were not well-captured by the model.

Model parameters were adjusted based upon this comparison and the model was subsequently used to predict the outcome of the quasi-static collision post load test. Agreement between model predictions and test results was lacking for this test. An extensive analysis of the test results and a series of post-test experiments ultimately revealed a design feature that adversely affected the ability of the post to deform, but was not captured by the model. The design of the end frame was modified based on this investigation.

Finally, the model was used to predict the outcome of the quasi-static corner post load test, which was conducted using the modified end frame design.

MODEL DEVELOPMENT

It is recognized that material failure is dependent not only on the extent that a material is strained beyond its yield point, but also on the nature of the stress that accompanies that strain. For example, materials generally can sustain much higher levels of stress in compression than they can in tension. Intuitively, a stress state that tends to pull a material apart tends to promote fracture of that material. This phenomenon is most often characterized through the triaxiality, Σ, of the stress state:

$$\Sigma = \sigma_m / \sigma_e ,$$

where σ_m is the mean stress (the average of the three principal stresses) and σ_e is the Mises stress (a measure of the magnitude of the stress).

Using the Bao-Wierzbicki criterion, failure initiates when the deformation of the structure induces plastic strain levels that exceed threshold values which are dependent on Σ, as illustrated in Figure 1. The solid line defines a plastic strain- and triaxiality-based failure envelope, in which damage initiates when the plastic strain exceeds the value defined by the curve. The unique shape of the line shown in Figure 1 is a fundamental characteristic of the Bao-Wierzbicki criterion. It is derived from a fit to the results of many tests that were conducted at different triaxiality levels, and accounts for the different modes of fracture that may occur, as indicated. It is also characterized by two parameters, C_1 and C_2, the fracture initiation strains for conditions of pure shear and uniaxial

tension, respectively. (Note that the C_1 and C_2 parameters are not independent—they are proportional and related to one another by a material hardening exponent [3].)

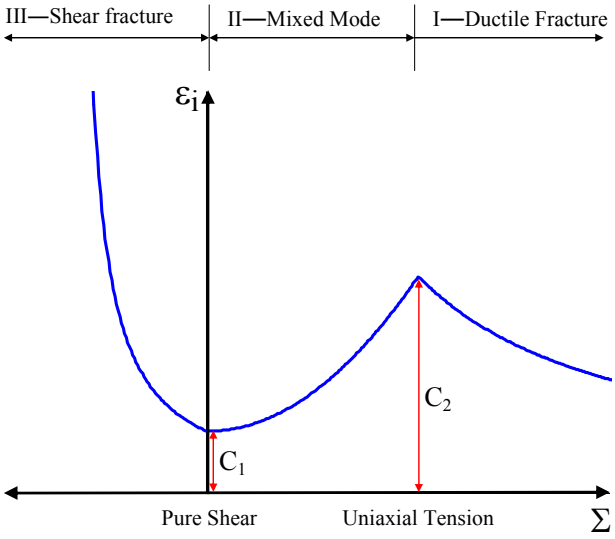

Figure 1. Schematic illustration of the Bao-Wierzbicki triaxiality-dependent failure initiation criterion.

The material model for the end frame structural elements was implemented in ABAQUS/Explicit using the Johnson-Cook plasticity model. The Bao-Wierzbicki failure criterion was defined using the '*DAMAGE INITIATION' material parameter option.

As is shown schematically in Figure 2, once failure initiates, the local strength of the material is assumed to decrease from its value at the fracture initiation strain, ε_i. The plastic strain at which the material strength decreases to zero is referred to as the failure strain, ε_f, as indicated in Figure 2. In ABAQUS, this behavior is defined through the '*DAMAGE EVOLUTION' material parameter. For reasons that are related to minimization of mesh-dependencies [12], the plastic strain at failure is described indirectly through definition of a plastic deformation at failure parameter, u_f. The strain rate, $\dot{\varepsilon}_{pl}$, following fracture initiation is defined to be proportional to the displacement rate $\dot{u}_{pl}$ such that:

$$\dot{u}_{pl} = L_e \bullet \dot{\varepsilon}_{pl},$$

where L_e is a characteristic length for elements near the location of fracture.

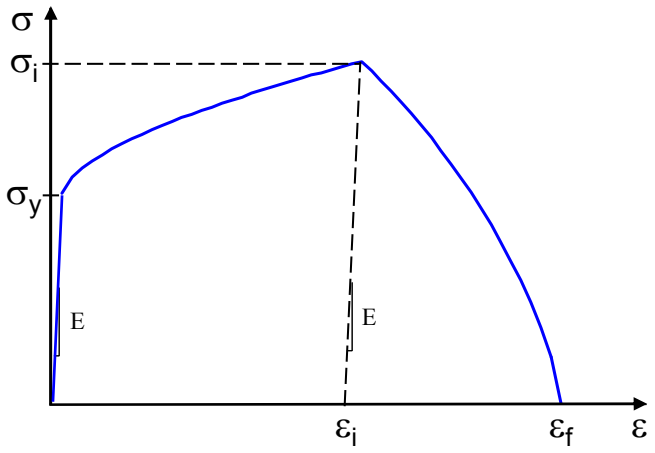

Figure 2. Stress-strain curve with damage evolution following initiation of material failure.

A test problem meant to be representative of the mechanics that govern the impact of a coil-shaped object into a corner post or collision post, was chosen to evaluate several aspects of the material failure model and determine how best to apply the model to the simulations of the full-scale tests. A schematic of the test problem is shown in Figure 3. In this problem, the transverse impact of a 48-inch diameter rigid coil moving at 21 mph into the center of a 76-inch-high post, fully-supported at both ends, is simulated. (Symmetry allows for modeling of only 1/4 of the beam.) Despite the simplified nature of the test problem, the all-solid mesh illustrated in Figure 4, which has only four elements through the thickness of the post members, uses over 220,000 elements. It would not be practical to create an entire endframe model using solid elements. Note that, following [7], elements with equal lengths in all dimensions (e.g. cubic-shaped for solid elements and square-shaped for shell elements) were used when modeling material failure.

Due to the practical numerical limitations of solid-only models, the use of shell-to-solid coupling was next investigated. This method, used by Tang, et al. [10], in the tank car impact study, allows for the use of solid elements in the area around the failure location and shell elements away from the failure location. With the interface of the solid-meshed and shell-meshed regions of the structure properly defined, appropriate kinematic constraints are automatically applied. Studies were conducted to evaluate the effect of: the size of the solid-element region, and the refinement of the mesh.

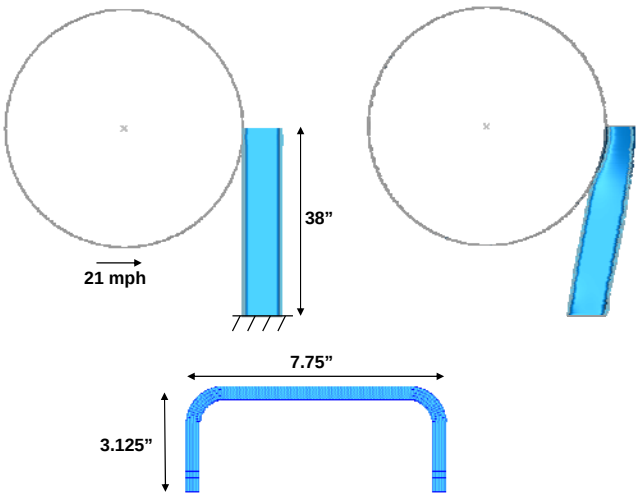

Figure 3. Schematic illustration of the coil impact test problem.

The results of these studies indicate that the size of the solid region needs to be large enough so fracture processes do not interact with the solid-to-shell interface. Otherwise, the results are not strongly affected. For example, if the solid region is 6.25 inches high, the predicted energy absorbed by the post prior to fracture is only about 2.5-percent higher than it is when the solid region is 3.125 inches high. Meanwhile, the number of elements in the mesh drops significantly. On the other hand, an evaluation of the effect of mesh density indicates that increasing the number of elements through the thickness of the post members from 4 to 8, as shown in Figure 4, decreases the energy absorbed at fracture by over 20 percent.

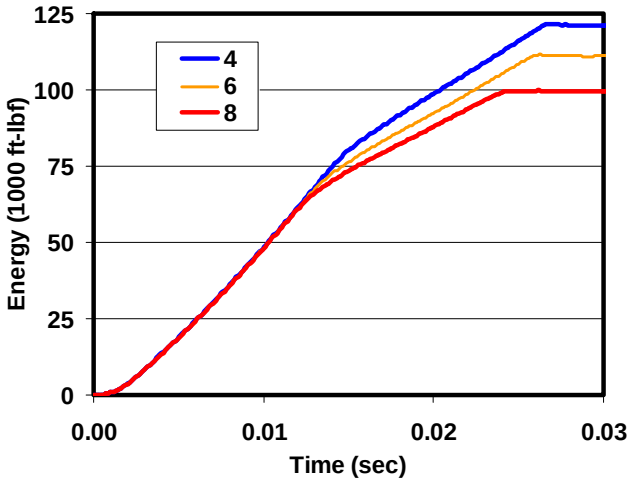

Figure 4. The effect of mesh refinement on the time-history of energy absorption for the test impact problem. The number of elements through the thickness of the post members is indicated.

Based on a preliminary investigation, we found the need for a refined mesh in the regions of failure, coupled with the potential for multiple failure sites, makes shell-only meshes more attractive than mixed solid/shell meshes for modeling the impact and large deformation of cab car end structures. In addition, some of the interfaces between structural elements are quire complex, and the connections between the collision and corner posts and the end beam are gusseted. The presence of the gussets makes it difficult to define the kinematic constraints at the shell/solid interface.

The failure modeling capability for ductile metals can be used with any ABAQUS elements that include mechanical behavior. Problems like the punch-through of the tank car head studied in [8–10] must be analyzed with solid elements, because the stress state during failure is dominated by through-thickness shear. However, when the structures are shell-like, and the stress in those structures is characterized by in-plane tension or compression, there is no inherent reason that shell elements cannot be used to model failure. One must take care that, when applying material parameters to use with shell elements, they been validated specifically for use with shell elements, because the stresses and strains that arise near the locations of failure are different for these two element types.

Validation of the Bao-Wierzbicki failure criterion, and any triaxiality-based criterion, for use with shell elements is complicated by the fact that the through-thickness stress is by definition equal to zero, for these elements. For this reason, the stress triaxiality is limited to the range -2/3 to +2/3. As long as the state of stress is truly biaxial, this does not appear to present any difficulties. However, in conditions where there is a sizable through-thickness stress, the definition of the triaxiality dependence of the failure initiation strain becomes difficult. This situation arises when, for example, the region of failure is near a relatively rigid connection, such as at the connection between the bottom of a collision or corner post and the end beam. For example, even with a great deal of mesh refinement, a shell element model may not pick-up what is likely to be an increase in the through-thickness stress just near a rigid connection, where failure may initiate. (It is worth noting that solid element models are likely to have similar issues at rigid connections.)

To evaluate the use of a shell element-only model with material failure, the solid or mixed solid/shell mesh for the coil impact test problem was replaced with a shell-only mesh with the same characteristic element size–0.09 inch. Initial calculations using identical failure parameters indicated that the shell-only model predicts a level of energy absorption that is about 45 percent less than the corresponding mixed solid/shell model. Inspection of the region where failure first initiates, as shown in Figure 5, reveals that the plastic strain distribution in the solid/shell and shell-only models is similar, but the peak strain levels are higher (30 percent vs. 15 percent) for the shell-only models, due to the manner in which the loads are accommodated.

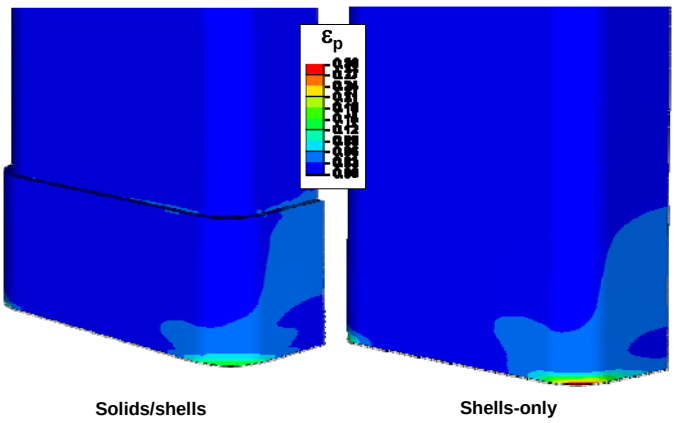

Figure 5. Comparison of strain distributions in solid/shell and shell-only models at base of post just prior to fracture initiation.

In addition to the different peak plastic strain levels, the triaxiality of the stress state in this region is different for the two types of models, as illustrated in Figure 6. In both types of models, the triaxiality builds-up and maintains a fairly constant level through the failure process. However, the level of triaxiality is significantly higher for the shell-only model.

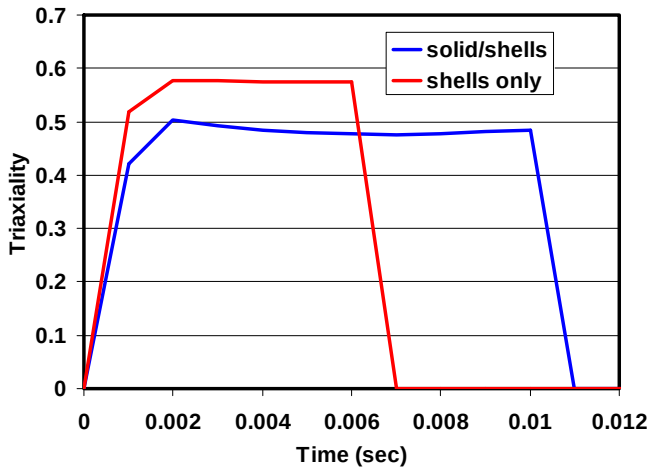

Figure 6. Comparison of triaxiality histories at the location of failure initiation for the solid/shell and shell-only models.

Because of the higher strain and triaxiality levels, complete failure of the post occurs much earlier in the shell-only models, thus the significantly smaller energy absorption. However, if the key Bao-Wierzbicki parameters C_1 and C_2 are modified (recall that they are proportional to one another), effectively raising or lowering the threshold failure curve shown in Figure 1, the behavior of the solid/shell and shell-only models can be made to be nearly identical. Figure 7 compares the deformation of the post for both a solid/shell model and a shell-only model just prior to complete failure and reveals that the deformed shapes are essentially identical.

The failure models for these two cases differ only by the magnitude of the C_1 and C_2 parameters. For this comparison, the C_2 parameter was set at 0.45 for the shell-only model, and 0.19 for the solid/shell model (the C_1 parameters were scaled accordingly). The energy absorption time-histories are also consistent, as shown in Figure 8. It is worth noting that the value of the C_2 parameter used in both models is significantly lower than value of 1.08 which was experimentally-determined for A710 steel [11].

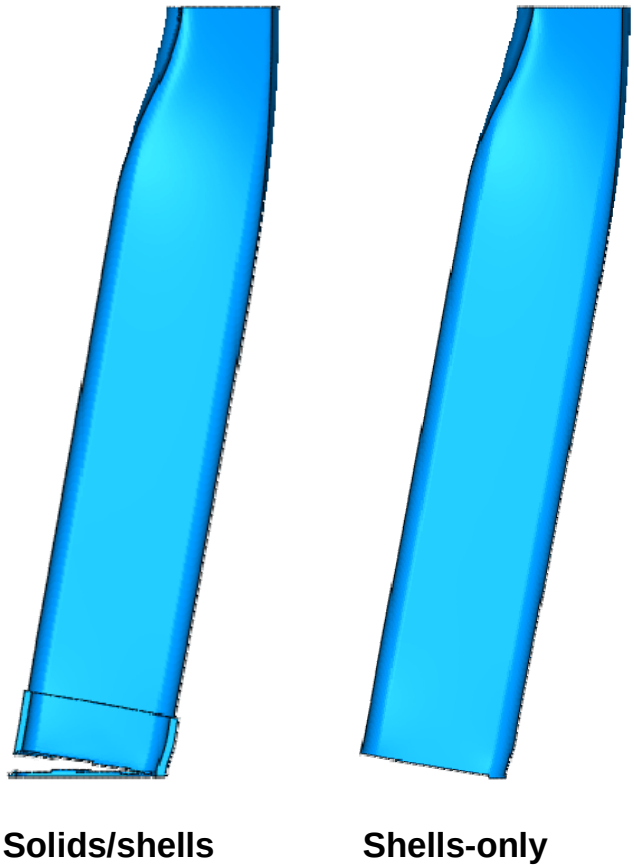

Figure 7. Comparison of post deformation just prior to complete failure for the solid/shell and shell-only models.

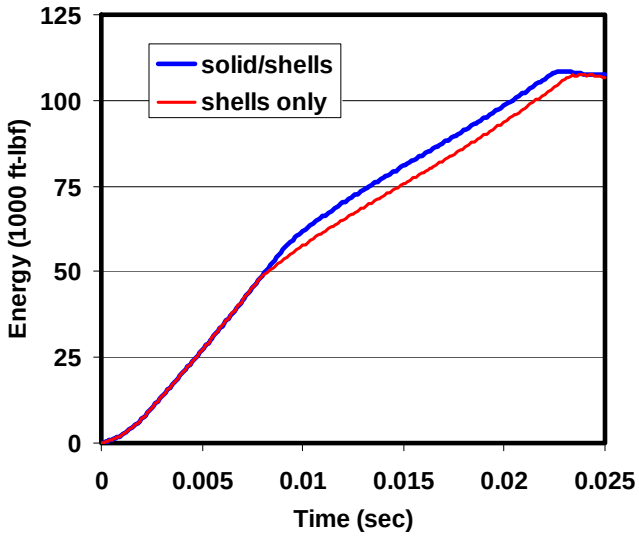

Figure 8. Comparison of post energy-absorption time-histories for the solid/shell and shell-only models.

MODEL VALIDATION

A shell-only model of the cab car end frame was constructed, and is pictured in Figure 9. The model contains approximately 160,000 elements, with an element size of approximately 1 inch away from the regions where failure may occur. The mesh is refined to an element size of 0.125 inch in the failure regions. The remainder of the vehicle was assumed to behave as a rigid mass. Preliminary calculations demonstrated that this assumption resulted in only minor changes to model predictions. Material failure parameters were adjusted by comparison to the results of the dynamic coil impact test of the corner post of the SOA end frame, which was conducted at TTC in June 2002 [5]. The corner post of the SOA end frame deflected about 10 inches due to impact of a 40,000 lbm, 6-foot diameter by 4-foot wide steel coil traveling at 14 mph, with the post fracturing in a few locations, but remaining attached to the end frame. A photograph of the base of the post following the test is shown in Figure 10.

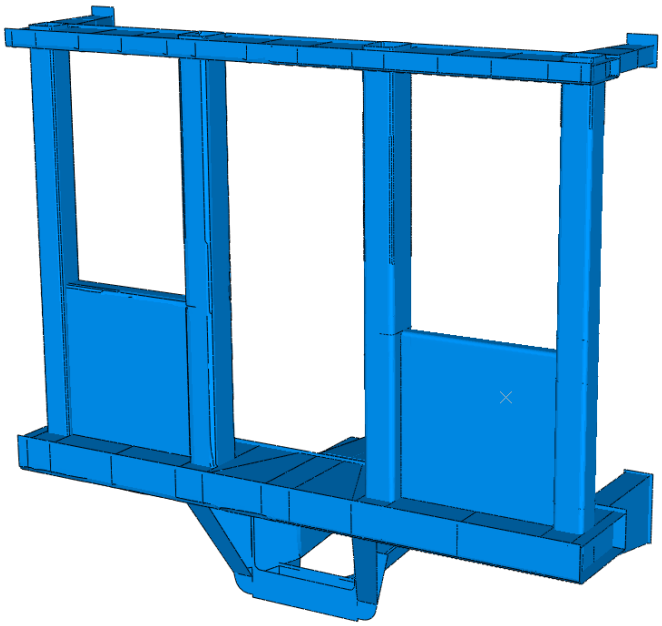

Figure 9. The finite element mesh for the cab car endframe.

Figure 10. Post-test photograph of base of corner post following coil impact.

Using measured material parameters for A710, the material from which the end frame was constructed, material failure parameters (namely, failure initiation parameters C_1 and C_2, and the plastic deformation at failure parameter, u_f) were modified to best capture the extent of fracture at the base of the post. The deformed end frame mesh following the simulated impact is shown in Figure 11 and is consistent with the extent of fracture and deformation shown in Figure 10.

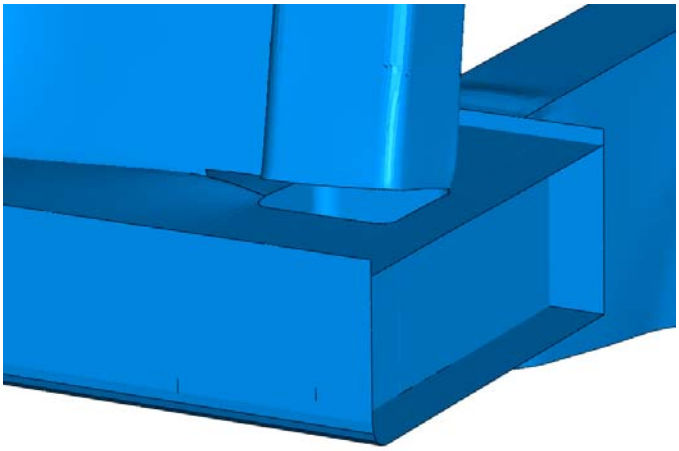

Figure 11. Predicted deformation of end frame following coil impact.

The predicted force-time history is compared with measured data in Figure 12 and appears to be consistent with test results. The predicted penetration of the coil is about 10.8 inches, as compared with 10.2 inches that were measured.

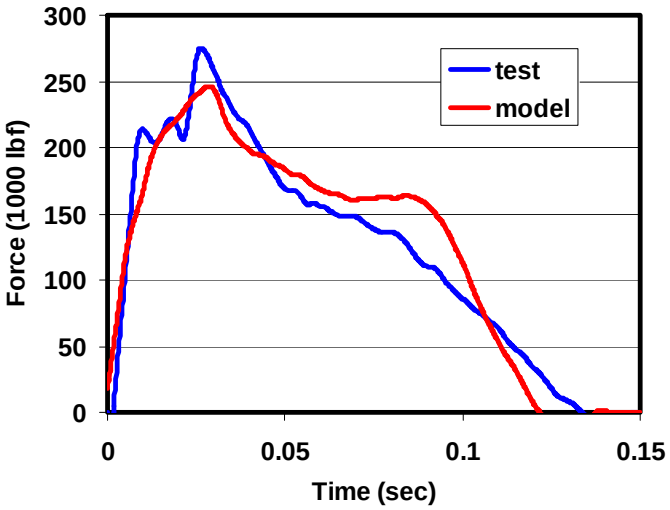

Figure 12. Comparison of predicted and measured coil force-time histories.

COMPARISON WITH RECENT TESTS

With the material parameters fit to the results of the 2002 test, the model was used to predict the results of the three additional full-scale tests which were performed in 2008. Schematic illustrations of the configurations for the single dynamic and two quasi-static tests are shown in Figures 13 and 14.

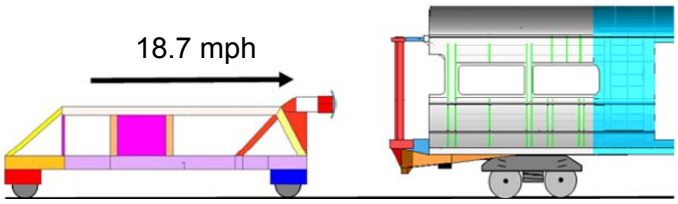

Figure 13. Schematic illustration of the dynamic impact test.

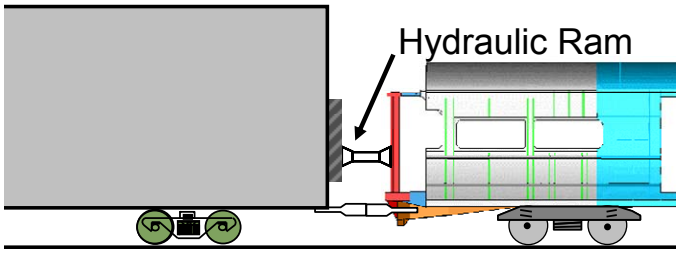

Figure 14. Schematic illustration of the quasi-static test.

For the dynamic test (Figure 13), a cart mounted with a coil shape was developed as an alternative to the steel coil resting on a frangible table used in the 2002 test. The striking surface at the front of the cart is rounded, with a 48-inch diameter and a width of 36 inches. It is positioned at the required height of 30 inches above the floor of the cab car, and centered on a collision post. The finished cart weighed approximately 14,000 lb, and the cab car weighed about 70,000 lb. The measured impact speed was 18.7 mph.

For the quasi-static test (Figure 14), the test car is coupled to a reaction car. Load is applied to a single collision or corner post through a hydraulic ram that is suspended from a crane. The load is reacted through the couplers of the two vehicles, with the draft gears replaced with rigid steel blocks. The applied force is measured using a set of four load cells positioned in series with the ram. Displacement is measured at a number of locations using string potentiometers.

Dynamic Collision Post Impact Test

The dynamic collision post impact test was conducted in April 2008. Pre-test model predictions of this test indicated that fracture would occur at the front base of the collision post, at its connection to the end frame, much like it did for the corner post test. A photograph taken following the test, shown in Figure 15, shows that the post fractured not only at the front base of the post, as predicted, but also at the rear of the post, behind the point of impact.

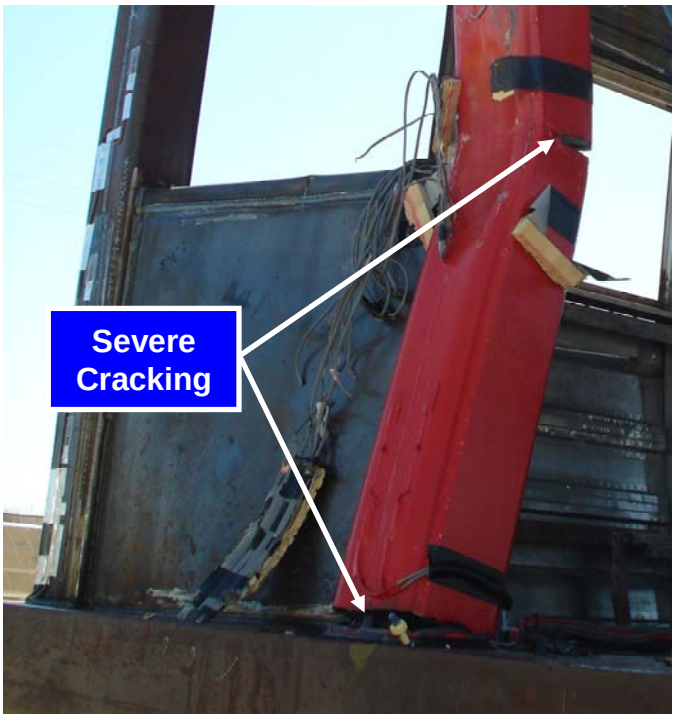

Figure 15. In the dynamic impact test, fracture occurred at the front base of the post and at the back of the post, opposite the point of impact.

An inspection of the fracture at the back of the post following the test revealed that it occurred at a location where both an internal gusset and an external tab are welded to the post. The fracture, in fact, occurred right along the edge of one of the two welds. These details, which were not in the original model, were subsequently added and the analysis was run again. The C_1 and C_2 parameters were again adjusted so the extent of fracture was consistent with the test results. With these changes, the calculated extent of fracture and deformation of the post was consistent with test results, as illustrated in Figure 16. Note that the material used to fabricate the collision posts is A572-50. This material exhibits ductility limits that are similar to, but not the same as, A710. Strength data used in the model were based on certifications provided with the A572-50 plates from which the collision posts were fabricated. It was necessary to extrapolate these data to form a complete stress-strain curve for this material. It is likely that much of the difference between the failure parameters found to be optimal for modeling A572-50 behavior in this test and those that were found to be optimal for modeling A710 behavior during the 2002 corner post impact test is attributable to differences in the hardening behavior assumed for the respective material models.

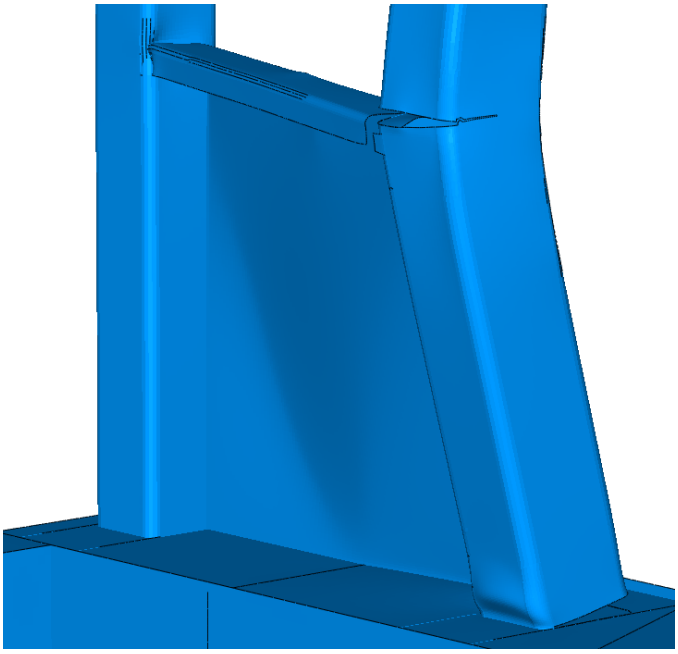

Figure 16. Predicted deformation of the collision post following the dynamic collision post impact (revised model).

Quasi-Static Collision Post Crush

The model was then used to predict the results of the quasi-static collision post test. As shown in Figure 17, the model predicted that the load would rise to about 260,000 lbf after 3 inches of post displacement, and then fracture would initiate at the front base of the post. Fracture at the back of the post was not expected to occur until after about 8 inches of post displacement.

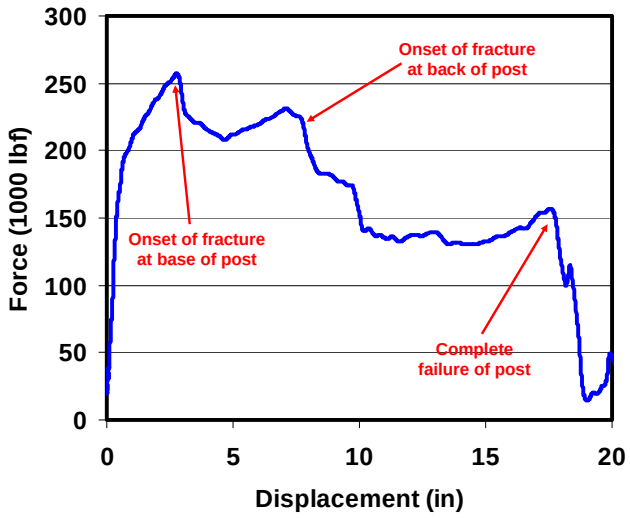

Figure 17. Predicted force-displacement curve for the quasi-static collision post load test.

Instead, as shown in Figure 18, fracture occurred first at the back of the post at a load of about 215,000 lbf after only about two inches of displacement. Fracture at the front base of the post initiated after approximately 2 more inches of displacement. Overall, the deformation behavior observed during the test was considerably different than the model predicted it would be.

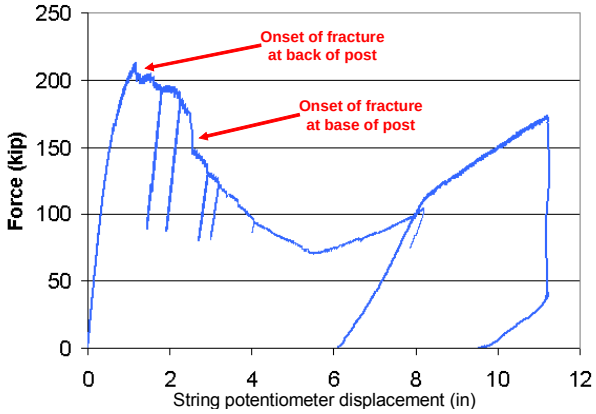

Figure 18. Measured force-displacement curve for the quasi-static collision post load test.

As a result of the poor behavior observed in this test, an investigation of the causes of premature fracture at the back of the post was initiated. The strength of the welds and the ductility of the material in this region were evaluated and determined not to be significant factors. It was eventually determined that the rigidity imparted to the post by the internal gusset and the strap that ties the back of the shelf into the back of the collision post, placed severe limitations on the ability of the post to deform in this region, with the net result being that it behaved in a relatively brittle manner, despite the fact that the A572-50 material the post is constructed from is quite ductile. Based on this evaluation, the shelf that connects the collision and corner posts was modified so it was not as deep, and would connect to the side of the posts rather than their back, as shown in Figure 19. The internal gusset was removed.

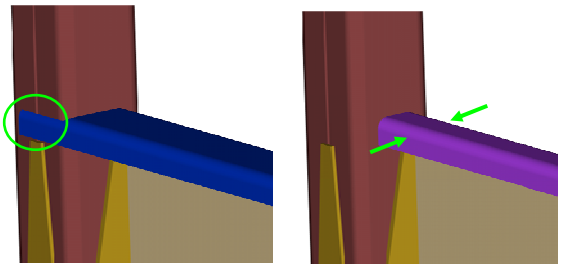

Figure 19. Schematic illustration of modifications to shelf connecting collision and corner posts.

Quasi-static Corner Post Crush

The model was revised to reflect the changes that were made to the design of the shelf, and the removal of the internal gusset, and was then used to predict the results of the quasi-static corner post crush test. The results of this test are compared with model predictions in Figure 20, and indicate that the predicted behavior is quite consistent with test results. Failure at the front base of the post was predicted to occur after 5 inches of crush. Test results indicate that the failure occurred at the base of the post after about 4.5 inches of crush. The measured energy absorption after 10 inches of post crush was almost exactly as predicted by the model. Post-test examination of the back of post, opposite the point of impact, reveals extensive deformation, but no fracture.

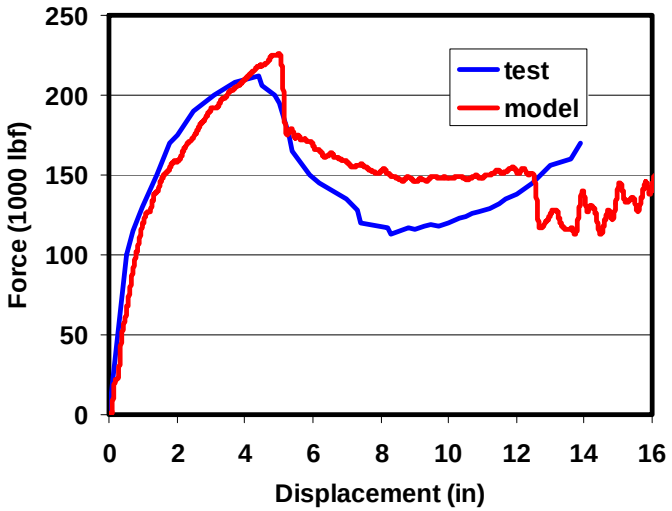

Figure 20. Comparison of predicted and measured force-displacement curves for the quasi-static corner post load test.

DISCUSSION AND CONCLUSIONS

A material failure model, based on the Bao-Wierzbicki criterion, was successfully implemented into ABAQUS for use with shell elements. Model development efforts indicate that the shell elements can be effectively used to model material failure. Moreover, it appears that the nature of the cab car end frame crush problem is such that the use of shell elements only is likely more effective than a mix of solids and shells.

The application of the model in simulations of the full-scale tests of cab car end frames demonstrates that material failure modeling can be an effective tool that increases the accuracy of pre-test predictions. For cases where fracture is likely, such models are very likely more accurate predictions of behavior than models that do not account for failure. It is evident, however, that there are potential pitfalls that must be avoided when evaluating model predictions. One lesson that was learned in this study is that these models lose much of their effectiveness when the fracture process is strongly influenced by complex structural details, such as the gusseted, strapped, and welded connection of the original design of the shelf connection to the collision post. In such cases, it may be difficult with shell elements only to capture important structural details that may have a significant effect on the

fracture behavior of the structure, and shell element-only models lose some of their effectiveness.

When such complexities are avoided, it appears as though, with some effort given to characterizing the failure properties of the materials and validating the material parameters, very effective models which account for material failure can be constructed and used to aid the design process and evaluate structural behavior.

One aspect of the problem that warrants additional study is the selection of the key failure parameters C_1 and C_2. It appears that when the failure parameters are optimized to predict failure at a connection (in our case, the front base of the post), they may not be optimal for failure in regions where there is no connection. In the model, the details of the connection are idealized, and the concentrated stress state that arises at the connection may not match the conditions in the actual structure. Away from connections, this issue isn't present, and it is more likely that the material parameters match measured values. For this same reason, there is likely to be more mesh-size dependence for a failure near a connection. Methods to account for such differences in conditions would allow the models to be less dependent on validation and therefore more widely applicable.

ACKNOWLEDGMENTS

This work was performed under contract to the Volpe Center as part of the Equipment Safety Research Program sponsored by FRA's Office of Research and Development. The authors sincerely appreciate the support and guidance offered by Michelle Muhlanger, technical representative for this program, as well as David Tyrell, Patricia Llana, and Benjamin Perlman of the Volpe Center. The authors also wish to thank Eloy Martinez and Luis Maal of FRA, Mark White and Tom Roderick of TTCI, and Ed Dunn of Zimmerman Metals, Inc.

REFERENCES

1. Notice of Proposed Rulemaking, "Passenger Equipment Safety Standards; Front-End Strength of Cab Cars and Multiple-Unit Locomotives, "49 CFR Part 238, Federal Register, Volume 72, No. 147, August 1, 2007, pp 42016–42041.
2. APTA SS-C&S-034-99, Rev. 2, "Standard for the Design and Construction of Passenger Railroad Rolling Stock", Vol. II—Construction and Structural, pp 11.0–11.44, American Public Transportation Association, 2003.
3. Bao, Y., Wierzbicki, T, "On Fracture Locus in the equivalent strain and stress triaxiality space," International Journal of Mechanical Sciences, 46, pp 81-98, 2004.
4. Mayville, R., Stringfellow, R., Martinez, E., "Development of Conventional Passenger Cab Car End Structure Designs for Full-Scale Testing, "U.S. Department of Transportation, DOT/FRA/ORD-06/20, December 2006.
5. Martinez, E., Tyrell, D., and Zolock, J., "Rail-Car Impact Tests with Steel Coil: Car Crush," Proceedings of ASME/IEEE Joint Railroad Conference, Paper No. JRC2003-1656, April 2003.
6. Priante, M., Llana, P., Jacobsen, K., Tyrell, D., and Perlman, B., "A Dynamic Test of a Collision Post of a State-of-the-art End Frame Design," American Society of Mechanical Engineers, Paper No. RTDF2008-74020, September 2008.
7. Yu, H., Jeong, D.Y., Gordon, J.E., Tang, Y.H., "Analysis of Impact Energy to Fracture Un-Notched Charpy Specimens Made from Railroad Tank Car Steel," Proceedings of the 2007 ASME Rail Transportation Division Fall Technical Conference, RTDF2007-46038, September 2007.
8. Tang, Y.H., Yu, H., Gordon, J.E., Priante, M., Jeong, D.Y., Tyrell, D.C., Perlman, A.B., "Analysis of Full-Scale Tank Car Shell Impact Tests," Proceedings of the 2007 ASME Rail Transportation Division Fall Technical Conference, RTDF2007-46010, September 2007.
9. Tang, Y.H., Yu, H., Gordon, J.E., Jeong, D.Y., Perlman, A.B., "Analysis of Railroad Tank Car Shell Impacts Using Finite Element Method," Proceedings of the 2008 IEEE/ASME Joint Rail Conference, JRC2008-63014, April 2008.
10. Tang, Y.H., Yu, H., Gordon, J.E., Jeong, D.Y., "Finite Element Analyses of Railroad Tank Car Head Impacts," Proceedings of the 2008 ASME Rail Transportation Division Fall Technical Conference, RDTF2008-74022, September 2008.
11. Lee, Y.-W., "Fracture Prediction in Metal Sheets," Ph.D. Dissertation, Department of Ocean Engineering, Massachusetts Institute of Technology, February 2005.
12. ABAQUS User's Manual, Version 6.8; Volume III: Materials; Chapter 20: Progressive Damage and Failure.